

# A Fourier–Shannon approach to closed contours modelling

Claudia Bonciu<sup>†</sup>, Christophe Léger<sup>‡</sup> and Jacques Thiel<sup>§</sup>

LESI (Laboratoire d'Electronique Signaux Images) et GDR PRC-ISIS du CNRS, Université d'Orléans, 12 rue de Blois, BP 6744, 45067 Orléans Cedex 2, France

Submitted 4 November 1997, accepted 25 June 1998

**Abstract.** This paper describes a modelling method for continuous closed contours. The initial input data set consists of two-dimensional (2-D) points, which may be represented as a discrete function in a polar coordinate system. The method uses the Shannon interpolation between these data points to obtain the global continuous contour model. A minimal description of the contour is obtained using the link between the Shannon interpolation kernel and the Fourier series of polar development (FSPD) for periodic functions. The Shannon interpolation kernel allows the direct interpretation of the contour smoothness in terms of both samples and Fourier frequency domains.

In order to deal with deformation point sources, often encountered in active modelling techniques, a method of local deformation is proposed. Each local deformation is performed in an angular sector centred on the deformation point source. All the neighbouring characteristic samples are displaced in order to minimize the oscillations of the newly created model outside the deformation sector. This deformation technique preserves the frequency characteristics of the contour, regardless of the number and the intensity of deformation sources. In this way, the technique induces a frequency modelling constraint, which may be subsequently used in an active detection and modelling environment.

Experiments on synthetic and real data prove the efficiency of the proposed technique. The method is currently used to model contours of the left ventricle of the heart obtained from ultrasound apical images. This work is part of a larger project, the aim of which is to analyse the space and time deformations of the left ventricle. The 2-D Fourier–Shannon model is used as a basis for more complex three-dimensional and four-dimensional Fourier models, able to recover automatically the movement and deformation of the left ventricle of the heart during a cardiac cycle.

**Keywords:** 2-D deformable model, Shannon interpolation, Fourier–Shannon modelling, Fourier filtering, ultrasound imaging

## 1. Introduction

The currently available automatic segmentation algorithms are not sufficiently powerful for many image classes. This is frequently the case in ultrasound imaging of the heart. For example, it is often necessary to locate the endocardic wall of the left ventricle in an apical cross section (figure 1). The ultrasound echo may be lost in noise when the ultrasound beam is parallel with the ventricle boundary. Moreover, the ultrasound echo reveals virtual boundaries at the mytral valves level in several instances of the cardiac cycle. In these cases, only an experienced

operator is able to locate the contour of the left ventricle. The expert interpolates the endocardic contour in those areas where it is indistinguishable, relying on his knowledge of the morphology of the ventricular cavity, especially of its overall shape. Despite recent progress reported in the literature [1–12], there is no general method for automatic boundary detection that provides satisfactory results in these cases. Most of the detection methods use specific *a priori* information about the characteristics of the target contours to solve the detection problem. The *a priori* information is also essential when the aim is to track motion within a sequence [11], particularly in order to obtain a three-dimensional (3-D) reconstruction of objects using these contours [13–21].

In this paper, we propose a deformable 2-D model that includes *a priori* information about the detected contour

<sup>†</sup> E-mail address: bonciu@lesi.univ-orleans.fr

<sup>‡</sup> E-mail address: leger@lesi.univ-orleans.fr

<sup>§</sup> E-mail address: thiel@lesi.univ-orleans.fr

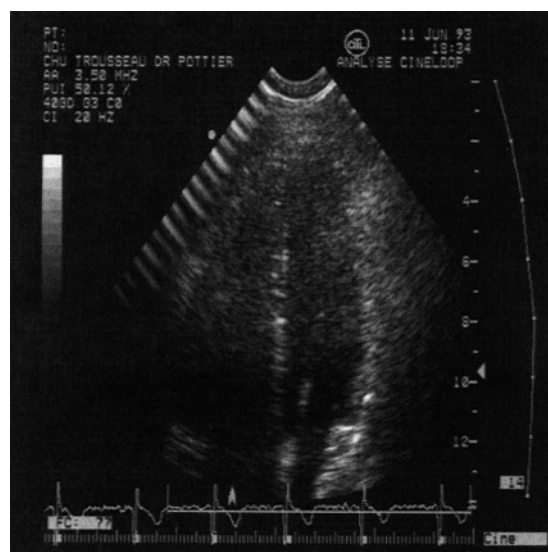


**Figure 1.** Four-cavity apical ultrasound image of the heart.

shapes. The information is expressed by the number of Fourier coefficients retained from the Fourier series of polar development (FSPD) of the contour samples. The modelling technique is valid for contours, which have an inner origin from which every radius crosses the contour in only one point. The model is based on the FSPD of the contour samples, which depends on the associated development origin. This origin (named central origin) is defined as the centre of the largest circle that approximates the contour by the least-squares method. The parameters of the model are the central origin coordinates and the Fourier coefficients of its polar development around this origin. A continuous contour is deduced from the model, using circular Shannon interpolation between the samples. The Shannon interpolation is optimal in the frequency domain [22]. Specifically, the Shannon interpolation provides the minimal frequency description in terms of number of Fourier coefficients. In this context, the number of Fourier coefficients directly defines the smoothness of the contour model.

The Fourier–Shannon technique provides an efficient way to deal with both discrete and continuous contours. This is a significant advantage when the modelled contours are used in subsequent 3-D and 4-D models. In this case, the continuous contour must be sampled following external geometrical constraints. Conversely, the image is usually considered a discrete map, and an active model is more conveniently expressed during deformation using a finite set of characteristic samples.

The Fourier–Shannon approach gives a global contour model. In order to deal with the active modelling environment, a deformation technique is proposed, which assumes that the image matching information is performed locally and gradually. The deformation technique restricts the spatial deformation to an angular segment centred on

the deformation source, while preserving the harmonic complexity of the modelled contour during the deformation process.

The first step of the modelling process selects the number of parameters of the model, using a representative set of reference contours. If necessary, the initial data points are locally smoothed and interpolated in order to obtain a closed continuous contour. Then, the number of modelling parameters is chosen to give the maximum degree of global smoothing (which corresponds to a minimal description model) constrained by a modelling error tolerance threshold. We use an undersampling iterative procedure, which measures the sampling error between two successive contour models, obtained with a different number of samples. Thus, this step provides a primary model, with the smoothness fixed by the number of FDSP coefficients.

This modelling step is performed using a representative selection of images, considering specific target reference contours. The choice of the number of parameters for the model is an important modelling issue. The proposed technique is sufficiently general to cope with the diversity of geometrical shapes that the modelling context may reveal during an automatic detection procedure. The use of this Fourier–Shannon model eliminates any direct geometrical restriction that may be contradictory with the (unknown) shape of a detected contour from the same class.

The second step consists in adjusting the values of the Fourier coefficients following an external deformation source, within angular sectors. The deformation process starts with an imposed deformation source, given by the image information detection procedure (a human expert or a features detection algorithm). This deformation is propagated to the neighbouring samples of the actual contour, in the angular sector centred on the initial deformed sample. The propagation law is designed to minimize the model contour oscillation outside the deformation sector, keeping the same harmonic complexity for the deformed contour. In this way, the continuous contour remains consistent with the initial frequency model after deformation.

The neighbouring samples are moved radially, within the defined sector. The oscillations outside the sector are the effect of the specific harmonic constraint expressed implicitly by the Shannon interpolation kernel. By imposing a maximum amplitude for these oscillations, the global smoothness given by the number of parameters of the model is guaranteed. A value over this amplitude indicates a breakdown of the model, which can be corrected by increasing the number of parameters of the model, or by enlarging the deformation sector. This technique provides a flexible way to deal with different modelling contexts, and is simple to use once the deformation propagation law has been established.

In principle, as well as in implementation, the proposed method uses several properties of circular

Shannon interpolation, which are presented in section 2. The iterative algorithm that determines the parameters of a contour model, for a specific class of target contours, is detailed in section 3. Section 4 presents the radial deformation technique used to adjust the contours following local image information. Finally, in section 5, two application examples of the proposed technique are described, in order to obtain the contours of the heart left ventricle models using ultrasound images.

## 2. Circular Shannon interpolation

### 2.1. Shannon interpolation kernel for periodic functions

A continuous signal, band limited to  $B$  Hz, can be optimally reconstructed from its samples using the well known Shannon interpolation theorem. The reconstruction is error-free when the samples are obtained at a frequency greater than  $2B$ . Using a lower sampling frequency, the interpolated signal oscillates around the initial signal, passing through the sample points. The lower the sampling frequency, the greater the oscillations. A quantitative analysis is difficult, since the interpolation kernel is defined for an infinite number of samples. This is not the case for periodic signals since both optimal reconstruction and measurement of the sampling error is possible using only the samples of one period. In [23], Schanze deduced a finite support Shannon kernel for periodic signals. This particular case will be detailed here, considering the polar contour development around an internal origin as a periodic continuous signal.

Let  $\rho(\theta)$ , with  $0 \leq \theta < 2\pi$ , represent this polar development. The  $2\pi$  periodic expansion of  $\rho(\theta)$  is a positive and continuous function  $\rho^\infty(\theta)$ .  $\rho^\infty(\theta)$  has a number  $M$  of Fourier coefficients  $\{C_m\}$ . Optimal sampling produces  $N = 2 \times (M - 1)$  samples  $\{\rho_n\}$  of  $\rho(\theta)$ , which are equiangular distributed along the contour,

$$\{\rho_n = \rho(n\Delta\theta)\} \quad (1)$$

with  $0 \leq n < N$  and  $\Delta\theta = 2\pi/N$ , and an infinity of periodic ( $N$ ) samples  $\rho_n^\infty$  of  $\rho^\infty(\theta)$ ,

$$\{\rho_n^\infty = \rho(n\Delta\theta)\} \quad (2)$$

with  $-\infty < n < +\infty$ , so that  $\rho_n^\infty = \rho_{n \bmod N}$ . Shannon interpolation with this infinity of samples yields the well known equation [24, 25]

$$\rho^\infty(\theta) = \sum_{n=-\infty}^{+\infty} \rho_n^\infty w^\infty(\theta, n, N) \quad (3)$$

with

$$w^\infty(\theta, n, N) = \text{sinc} \left[ N \left( \frac{\theta}{2} - \pi \frac{n}{N} \right) \right] \quad (4)$$

where  $\text{sinc}(\cdot) = \sin(\cdot)/(\cdot)$ .  $\rho^\infty(\theta)$  is strictly equal to  $\rho(\theta)$ . The reconstruction requires, for each value of  $\theta$ , with  $0 \leq \theta \leq 2\pi$ , an infinite summation of  $\{\rho_n^\infty\}$  weighted by the classical sinc function.

The reconstruction is reduced to  $N$  samples  $\{\rho_n\}$ , distributed in a period that corresponds to a complete rotation of the polar angle, using the Shannon kernel for periodic functions [23]:

$$\rho^\infty(\theta) = \rho^N(\theta) = \sum_{n=0}^{N-1} \rho_n w^N(\theta, n, N) \quad (5)$$

where

$$w^N(\theta, n, N) = \frac{(-1)^n}{N} \sin \left( N \frac{\theta}{2} \right) \mathbf{F}_N \left( \frac{\theta}{2} - \pi \frac{n}{N} \right) \quad (6)$$

with

$$\mathbf{F}_N(\cdot) = \frac{1}{\tan(\cdot)} \quad \text{if } N \text{ is even} \quad (7)$$

and

$$\mathbf{F}_N(\cdot) = \frac{1}{\sin(\cdot)} \quad \text{if } N \text{ is odd.} \quad (8)$$

The periodic function Shannon interpolation (5) allows the finite summation of only the  $N$  samples  $\{\rho_n\}$  weighted by a new kernel function  $w^N$ . This new function is  $2\pi$ -periodic with respect to  $\theta$ , as illustrated in figure 2 in the particular case where  $n = 0$  and  $N = 16$ . At the limit, when the number  $N$  of samples is infinite, the kernel functions  $w^N$  and  $w^\infty$  become equal. When  $N$  is finite, they are quite close for  $0 \leq \theta \leq \pi$ , but become very different beyond this angular domain. Hence, reconstructing an optimally sampled closed contour is particularly simplified with the interpolation relation (5).

The study of the undersampling error is simplified for the kernel given by equation (6). However, an analytic expression of the sampling error is still difficult to obtain. In this paper, the numerical analysis was carried out using additional hypotheses, detailed in the following paragraphs.

When a contour  $\rho^N(\theta)$  is undersampled with  $K < N$  equiangular samples, the resulting reconstruction  $\rho^K(\theta)$  is obtained by circular Shannon interpolation by replacing  $N$  with  $K$  in (6) and using  $\Delta\theta = 2\pi/K$ . The  $\rho^K(\theta)$  is different from  $\rho^N(\theta)$  except for the  $K$  samples that are the intersection points of both contours. The sampling error function is defined using the  $L_1$  norm, as  $\varepsilon^K(\theta) = |\rho^N(\theta) - \rho^K(\theta)|$ . We define the maximum relative deformation tolerance as

$$\hat{\varepsilon}(K) = \max_n \left| \frac{\max_{\theta \in [n\Delta\theta, (n+1)\Delta\theta]} \varepsilon^K(\theta)}{\rho^K(\theta_{\varepsilon_{\max}}^n)} \right| \quad (9)$$

where  $\theta_{\varepsilon_{\max}}^n = \arg \max_{\theta \in [n\Delta\theta, (n+1)\Delta\theta]} \varepsilon^K(\theta)$  with  $0 \leq n < K$ .

Numerical simulations have shown that the maximum of the error function is often placed at the middle of the

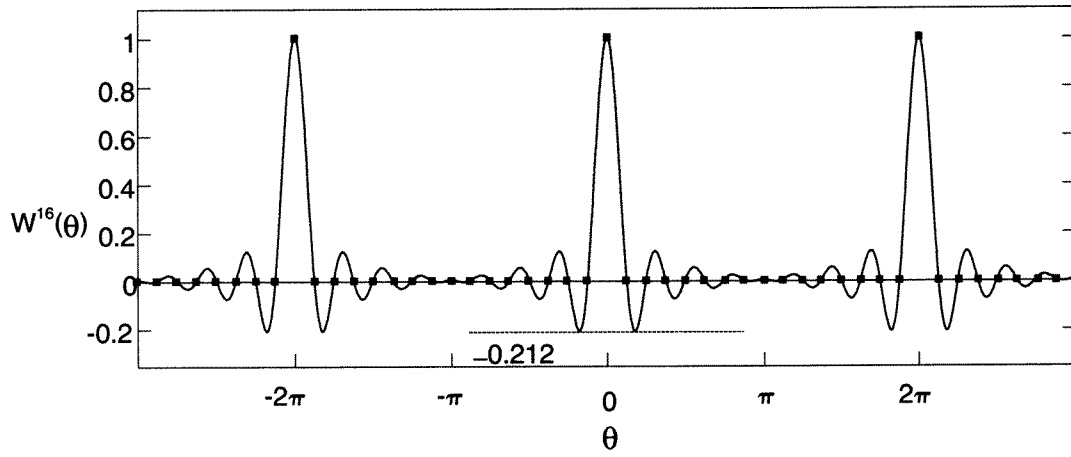


**Figure 2.** Shannon interpolation kernel for periodic functions  $w^N(\theta)$  for the case  $n = 0$  and  $N = 16$ .

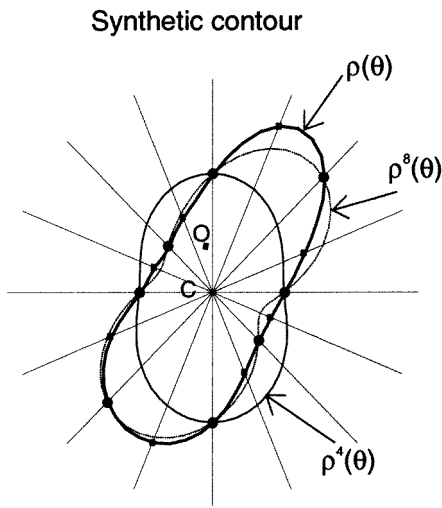


**Figure 3.** Synthetic contour  $\rho(\theta)$  and the contours  $\rho^4(\theta)$  and  $\rho^8(\theta)$  obtained by undersampling the  $\rho(\theta)$  function (with respectively four and eight samples).

sample interval. This was verified for a numerical grid of up to  $1/25$  of the sampling interval, with  $N \in [8, 128]$  and reasonable smooth synthetic contour models. With this hypothesis, a simplified form of (9) may be used:

$$\hat{\varepsilon}(K) = \max_n \left| \frac{\varepsilon^K([n + 1/2]\Delta\theta)}{\rho^K([n + 1/2]\Delta\theta)} \right| \quad (10)$$

with  $0 \leq n < K$ .

To illustrate this formula, the synthetic contour  $\rho(\theta)$  (figure 3) is considered. Its polar development around origin C is shown in figure 4. The contour is described with only nine Fourier coefficients (1.0, 0.0,  $0.25e^{i2\pi/3}$ ,  $-0.02$ ,  $0.06e^{i4\pi/3}$ , 0.02, 0.01,  $0.01e^{i\pi/3}$ , and 0.005) so that the optimal sampling is obtained with 16 equiangular samples ( $\varepsilon_C(16) = 0$ ). The effects of the undersampling oscillations

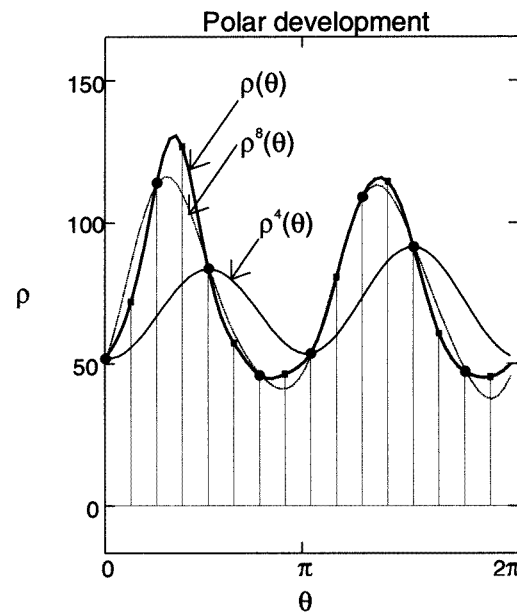


**Figure 4.** Polar development of the contours  $\rho(\theta)$ ,  $\rho^4(\theta)$ , and  $\rho^8(\theta)$ .

are outlined for the contours  $\rho^4(\theta)$  and  $\rho^8(\theta)$  in figures 3 and 4, using thin full and broken curves, respectively.

## 2.2. Fourier analysis and Shannon circular interpolation

The circular Shannon interpolation function can be computed using the discrete Fourier transform (DFT). Equation (3) is the convolution of the discrete contour polar development with the cardinal sinus function, i.e. a multiplication with a rectangular window in the frequency domain. An optimally sampled contour with  $N$  samples is completely characterized by its  $M$  complex Fourier coefficients  $\{C_0, \dots, C_{M-1}\}$ ,  $M = (N + \xi)/2$ , where  $\xi = 1$

if  $N$  is odd and  $\xi = 2$  if  $N$  is even. These  $M$  coefficients are directly deduced from the  $M$  first values  $\{S_0, \dots, S_{M-1}\}$  of the DFT of the sequence  $\{\rho_n\}$ ,  $0 \leq n < N$ , using the relations [26]:

$$C_m = \begin{cases} \frac{S_m}{N} & 0 \leq m < M-1 \\ \frac{1}{\xi} \frac{S_{M-1}}{N} & m = M-1 \end{cases} \quad (11)$$

where  $\xi = 1$  if  $N$  is odd and  $\xi = 2$  if  $N$  is even.

It can be deduced that the real part of the DFT of the sequence of dimension  $N$ , defined by  $\{S_0, 2S_1, \dots, 2S_{M-2}, 2S_{M-1}/\xi, 0, \dots, 0\}$  is the ideal sampling  $\{\rho_n\}$ ,  $0 \leq n < N$ , of the contour. This sampling can also be obtained by inverse DFT of the whole sequence  $\{S_0, \dots, S_{N-1}\}$ . Moreover, by padding the  $N$  values  $\{S_0, 2S_1, \dots, 2S_{M-2}, 2S_{M-1}/\xi, 0, \dots, 0\}$  with  $L$  zero samples,  $N+L$  values of the contour  $\{\rho(2\pi n/(N+L))\}$ ,  $0 \leq n < N+L$ , are obtained by inverse DFT. Thus, the initial signal samples can be reconstructed by circular Shannon interpolation by the inverse DFT of the sequence  $\{S_0, 2S_1, \dots, 2S_{(N/2)-1}, 2S_{((N+\xi)/2)-1}/\xi\}$  padded with as many samples as required.

Consider a continuous contour, optimally sampled with  $N = 2\eta$  equiangular samples ( $\eta$  is an integer). If this contour is undersampled by multiplying the sampling step  $\Delta\theta = 2\pi/N$  by two, the sampling error can be estimated using equation (10) with DFT twice. A direct DFT on  $N/2$  samples will give the sequence  $\{S_0, \dots, S_{(N/2)-1}\}$ . An inverse DFT on the sequence  $\{S_0, 2S_1, \dots, 2S_{(N/4)-1}, S_{N/4}\}$  padded with  $(3N/4) - 1$  zero samples will give the corresponding sample values for the angles  $n\Delta\theta$ ,  $0 \leq n < N$ . When  $n$  is even, these values coincide with the initial contour samples. When  $n$  is odd,  $N/2$  interpolated values are obtained at the middle of the sampling intervals. The maximum of the differences between these  $N/2$  values and those of the initial contour at the same angles gives, therefore, an estimation of the sampling error (10).

The DFT algorithms lead to dichotomies, useful for a fast estimate of the number of samples for a given target contour. This first estimation may be further refined, using the direct computation of the error (10) given by equations (5)–(8), when  $N$  or  $K$  are not dyadic numbers.

### 3. Fourier–Shannon model fitting

In this section, a general technique for deducing the Fourier–Shannon model parameters for a given class of the target contours is detailed. The Fourier–Shannon technique models a closed continuous contour using a minimum number of parameters. The necessary degree of smoothness, expressed in terms of the number of Fourier coefficients, is deduced using reference contours. The iterative technique detailed here emphasizes the signal processing approach. The selection of a representative

data set, the relevance of the reference contours, and the accuracy of the obtained model is application specific and must be treated with the standard pattern recognition methods [26].

The polar contour development depends on the choice of the polar origin. To estimate the polar (central) origin, which gives the minimum number of characteristic samples for a model contour, we use the iterative algorithm described in [27]. Once this origin is established, we try to deduce the minimum number of characteristic samples needed to fit a reference contour. This contour is obtained from a sufficiently accurate data set, with a sufficiently large number of characteristic samples.

#### 3.1. Global model estimation

We assume that the modelling error for the reference contour is small enough to be neglected. We use an iterative procedure, which starts with a small number of characteristic samples and increases this number at each step. A tolerance measure (10) is computed and iterations stop when the tolerance is lower than a prescribed threshold  $\varepsilon_T$ . At each step, the reference contour is  $k$ -sampled, and the new samples are calculated using DFT twice, as described in section 2.2, or using the direct implementation of the interpolation kernel (5)–(8) in section 2.1. The comparison between these  $k$  new values and those of the initial contour model at the same angles gives an estimation  $\hat{\varepsilon}_O(k)$  of the undersampling error defined by (10). If  $\hat{\varepsilon}_O(k)$  is greater than the threshold  $\varepsilon_T$ ,  $k$  is increased and the procedure is repeated until the current tolerance measure is less than  $\varepsilon_T$ . At the last iteration ( $k = K$ ), the contour is approximated with the required accuracy by the continuous contour deduced by circular Shannon interpolation between the  $K$  samples.

The threshold  $\varepsilon_T$  depends on the desired degree of accuracy for the specific application. A small value of the threshold  $\varepsilon_T$  will produce an accurate model, but the Fourier description will include a significant number of coefficients. Generally, the modelling quality is measured subjectively, and only an expert is able to establish, experimentally, if the tolerance threshold  $\varepsilon_T$  is small enough for the given application.  $\varepsilon_T$  is a relative measure and it must be related to the average radius of detected contours. For example, a 1% tolerance may give subpixel displacements for an average radius up to 100 pixels, but for smaller contour radii, a larger tolerance may be a better choice.

The above procedure is used to fit several reference contours, for representative images, and gives an initial estimate of the characteristic samples for a specific modelling context. As will be detailed in the next section, a breakdown of the model may be allowed during the deformation process, if this estimate model conflicts with the detected contour shape frequently.

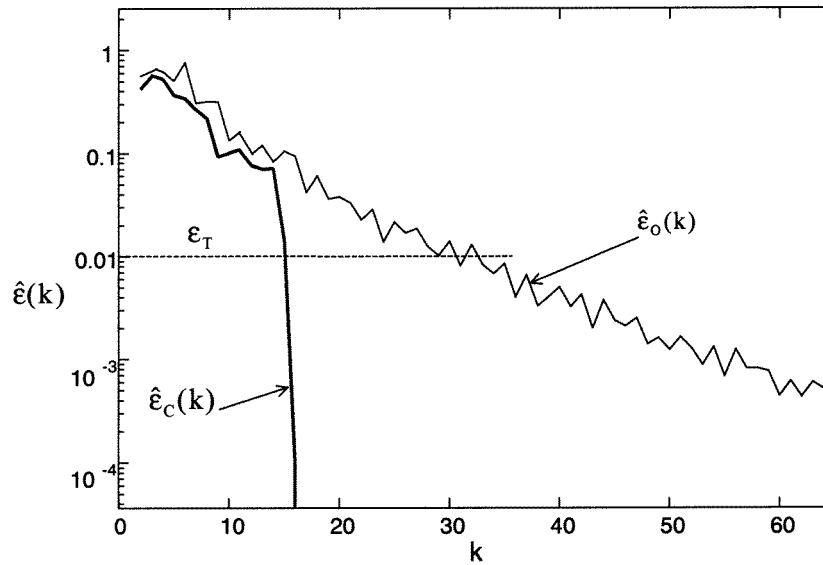


**Figure 5.** Variations of the estimation  $\hat{\epsilon}(k)$  of the sampling error with respect to the number of samples  $K$  for the synthetic contour of figure 3, sampled from origins O and C (central origin).

### 3.2. Polar development origin

The study of the sampling quality, as a function of the polar development origin, is important in this modelling context. To illustrate this point, the global modelling technique described above is used for the synthetic contour of figure 3. When this contour is developed around the internal origin O, which differs from the central origin C,  $K = 25$  samples are needed to obtain a tolerance  $\hat{\epsilon}_O(K)$  less than  $\epsilon_T = 1\%$  (instead of  $K = 15$  with origin C). Figure 5 shows that with the same number  $k$  of samples, the error  $\hat{\epsilon}_O(k)$ , computed in origin O, is always greater than the error  $\hat{\epsilon}_C(k)$ , computed using the polar development around the origin C ( $\hat{\epsilon}_O(16) = 9\%$  whereas  $\hat{\epsilon}_C(16) = 0$ ). As described in [27], the central origin corresponds to a zero value for the first Fourier coefficient  $C_1$ .

It has been numerically verified that the central origin produces smaller undersampling errors for quasi-circular contours. Unfortunately, an analytic proof of this property is not available for general contour shapes. The sampling error depends on the numeric values of all the contour samples. The minimization of this error with respect to the polar origin coordinates leads to a nonlinear optimization problem that can only be solved numerically in the general case. For a circular contour, the sampling error varies as a function of the distance  $\Delta\rho$  between the chosen origin O and the central origin C (appendix A) as

$$\begin{aligned} \epsilon(k, \Delta\rho) &= \max_n \left| 1 - \frac{1 + \sum_{m=0}^{k-1} (\Delta\rho/\rho_0) \cos(m\Delta\theta) w^N(\theta, m, k)}{1 + (\Delta\rho/\rho_0) \cos[(n + \frac{1}{2})\Delta\theta]} \right| \end{aligned} \quad (12)$$

with  $0 \leq n < k$  and  $0 < k \leq K$ .

This first-order approximation is true if  $\Delta\rho$  is well below the radius  $\rho_0$  of the circular contour. Our numerical simulations showed that this property of the central origin C remains true for almost circular contours, and, by extension, for the contours used here.

To take into account the central origin properties described above, the fitting algorithm is modified in order to approach the central origin C at each step. The central origin is the centre of inertia of the contour samples when the sampling is optimal [19]. Its coordinates are found by successively re-sampling the continuous contour, choosing at each step the centre of inertia of the samples at the previous iteration.

The Fourier–Shannon technique allows the description of a continuous contour model with  $N$  samples equally distributed around their centre of inertia. Alternately, the description is given in the frequency domain, by  $M = (N + \xi)/2$  complex Fourier coefficients<sup>†</sup>.

### 4. Local contour deformation

A local contour deformation is frequently encountered in active modelling techniques, which use local image information to iteratively adjust the contour shape, and finally obtain an energy-like function minimum [28]. Our aim is to allow this type of local contour deformation, while keeping the global model characteristics. We propose a technique that preserves the initial number of parameters of the Fourier–Shannon model, but adjusts their values to consider the deformations. Thus, we obtain a deformable model that is coherent with the initial harmonic hypothesis,

<sup>†</sup> Except the first one, which is always real, and the last one, which is real when  $N$  is even.

expressed by the number of characteristic samples or, alternatively, by the number of Fourier coefficients.

Global model consistency is an important issue for active contour detection methods. It is generally solved using boundary rigidity constraints. There is always a trade-off between elasticity and plasticity in an active contour model. Rigidity is usually expressed in additional energy terms, which depend on the contour sample displacements. These terms also play an important role in the deformation discrete time dynamics. Contour deformation stops when the equilibrium between the external (image features) energy and the internal (contour shape) energy is obtained. This can be a drawback, when the initial rigidity constraints are not appropriate to the image features map used to compute the deformation.

The proposed frequency domain constraints are better able to express scale invariant features and a rich variety of geometric shapes with few parameters. The samples of the modelled contour are linked by means of a global Fourier transform. The Fourier coefficient space is a heterogeneous space, because each Fourier coefficient has a different geometrical significance. Consequently, it is possible to define scale-invariant features for the modelled contours, by imposing weak constraints on the Fourier coefficients. For example, global elliptic eccentricity may be imposed using the ratio between the first two Fourier coefficients. This feature does not depend on the contour dimensions or on the ellipse orientation. A complete study of the geometric properties of the FSDP in the pattern recognition context will be the subject of a separate report.

In this paper, we treat the simplest case, when the constraint is imposed on the number of allowed frequencies of the model. Our primary concern here is to ensure a consistent linkage between different processing stages for a complex spatial–temporal model of the heart. To this purpose, the Fourier–Shannon model ensures that the modelled contours have the same spectral characteristics for all the images in a sequence.

The usual active modelling technique is considerably simplified in the context of global modelling constraints, since the external energy term is sufficient to sustain the deformation dynamics. This is possible only with a non-local elasticity constraint, as is the case of the Fourier–Shannon model. The usual elasticity constraints are imposed locally, in a neighbourhood of the deforming boundary, and are often used as deformation regulators [28–31]. Slightly different elastic constraints may produce significantly different deformations for the same information concerning image features. The proposed global model, which is obtained following an analysis of reference contours, implicitly induces an elasticity constraint. This is a major advantage when the pattern recognition analysis is the primary concern. Our approach gives priority to this point of view. Most of the deformation techniques encountered in the literature on active modelling [32–35] are sufficiently powerful to deal with predefined

elastic constraints. There are many possibilities to obtain a deformation dynamic regulation based exclusively on the extraction procedures for the features and on the specific constraints for the external forces. Consequently, a model-based, pre-defined elasticity constraint may be a better choice in complex detection problems, especially since such a constraint does not affect significantly the convergence of the active detection algorithm.

In the following, a local deformation technique is detailed, in order to integrate the Fourier–Shannon model in the active modelling context. An external deformation source imposes a radial displacement of a modelled contour. To keep the global model characteristics, the neighbouring samples included in an angular sector centred on the deformation source have to be displaced. The new sampling defines an interpolated contour, which usually oscillates outside the modified sector, around the initial contour. We study here how to obtain the weighting window for the samples contained in the deformed sector, so that the error between the two contours outside the sector does not exceed a maximum value  $\varepsilon'_T$ . This technique allows the deformation of the initial contour within several sectors, simultaneously and independently, since the modification introduced within a sector does not significantly change the contour shape in the outer angular sector. Several approximations must be made in order to simplify the deformation analysis. However, once the analysis is performed, the deformation control is reduced to a simple weighting operation.

Using the previous section notation, a modelled contour is expressed by its  $K$  polar coordinates  $(\rho_n, \theta_n)$ ,  $0 \leq n < K$ , where  $\rho_n$  are the vector radii and  $\theta_n$  are the angles of these radii. The radial displacement  $\Delta\rho_n$  of one sample, at the angle  $n\Delta\theta$ , defines a new contour  $\rho_n(\theta)$ . The distance  $\delta_n$  between the contours is obtained using (5) as

$$\delta_n = |\rho_n(\theta) - \rho(\theta)| = |\Delta\rho_n|w^N(\theta, n, N). \quad (13)$$

$\delta_n$  depends only on the distance of the displaced sample and on the Shannon interpolation kernel. The oscillation amplitudes decrease symmetrically from the diameter  $(n\Delta\theta)$ , as illustrated in figure 2, for  $n = 0$  and  $N = 16$ .

When two neighbouring samples at angles  $n\Delta\theta$  and  $(n+1)\Delta\theta$  are symmetrically displaced, the contour distance becomes

$$\delta_{n,n+1}(\theta) = |\Delta\rho_n|w^N(\theta, n, N) + |\Delta\rho_{n+1}|w^N(\theta, n+1, N). \quad (14)$$

Outside the sector defined by these two samples, both oscillations produced are in opposite phase, and the resulting oscillation amplitude is lower when both samples are displaced by the same distance  $\Delta\rho$ . The interpolation function is consequently maximum, between both displaced samples, at the angle  $\theta_{max} = (n + \frac{1}{2})\Delta\theta$ . Figure 6 represents the function  $\delta_{n,n+1}$  when  $N = 16$  and  $\theta_{max} = 0$ .

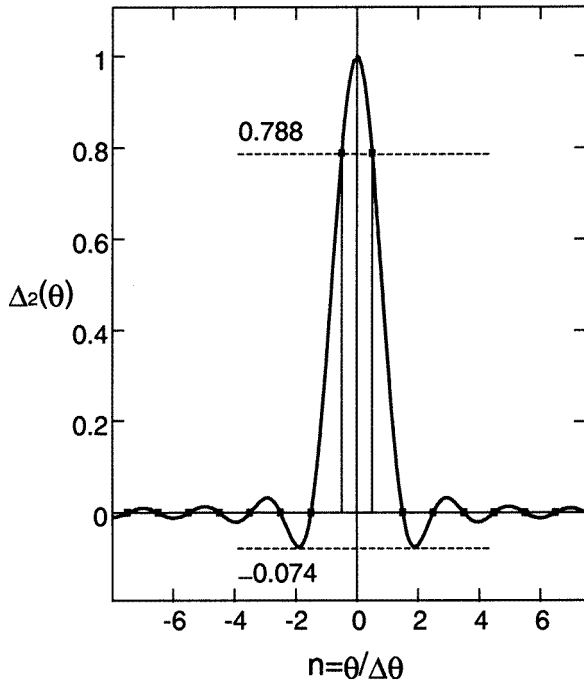


**Figure 6.** The function  $\Delta_2(\theta) = \delta_{n,n+1}(\theta)/\Delta\rho_n$ ,  $\Delta\rho_n = \Delta\rho_{n+1} = 0.788$ .

With  $\Delta\rho_{max} = 1$ , the amplitude of the displacement of both samples is equal to 0.788. The highest oscillation amplitude, equal to  $0.074\Delta\rho_{max}$ , is observed on either side of this maximum, for an angular distance of  $1.39\Delta\theta$ . The ratio of the maximum distance between contours, after and before adjustment, and the maximum oscillation amplitude is equal to 13.514.

The displacement of three samples can increase the ratio between the central deformation and the maximum oscillation amplitude if these oscillations counterbalance each other. The displacements of both lateral samples have to be equal. Hence, the ratio between this displacement and the central sample displacement has to be determined in order to minimize the maximum oscillation amplitude. This optimization problem has been solved numerically for  $N = 16$ : both lateral samples have to be displaced 2.35 times less than the central sample. This deformation is now 144 times greater than the maximum oscillation amplitude, detected at the angle  $2.219\Delta\theta$  relative to the central radius. The relative measure function  $\Delta_3(\theta) = \delta_{n-1,n,n+1}(\theta)/\Delta\rho_n$  is plotted in figure 7.

In the general case of  $K$  samples displaced in the deformation sector, the oscillations are minimized by a deformation vector  $\Delta\tilde{\rho} = [\Delta\tilde{\rho}_{-K/2}, \dots, \Delta\tilde{\rho}_0, \dots, \Delta\tilde{\rho}_{+K/2}]$ , considered as the solution of the optimization problem:

$$\begin{aligned} \Delta\tilde{\rho} &= \arg \min_{\theta \in \Omega} \max |\delta(\Delta\rho, \theta)| \\ &= \arg \min \left\{ \max_{\theta \in \Omega} \left| \sum_{i=-K/2}^{K/2} \Delta\rho_i w^N(\theta, i, N) \right| \right\} \end{aligned} \quad (15)$$

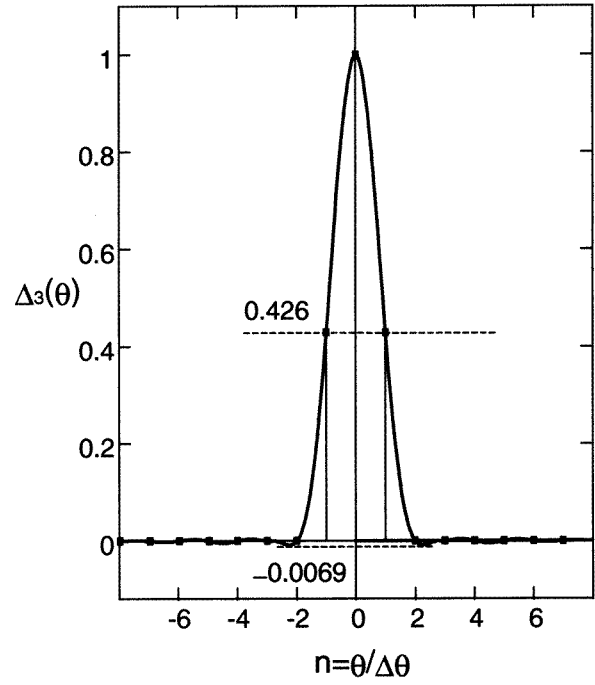


**Figure 7.** The function  $\Delta_3(\theta) = \delta_{n-1,n,n+1}(\theta)/\Delta\rho_n$ ,  $\Delta\rho_n = 1.000$ ,  $\Delta\rho_{n-1} = \Delta\rho_{n+1} = 0.426$ .

where

$$\Omega = \left[ \left( \frac{K}{2N} - 1 \right) \pi, -\pi \right] \cup \left[ \frac{K}{2N} \pi, \pi \right]$$

is the outer deformation window sector. The deformation window symmetry generates the optimization constraints  $\Delta\rho_{-i} = \Delta\rho_{+i}$ ,  $i = 1, \dots, K/2$ . The properties of the interpolation kernel do not allow an analytic solution of the problem, even for  $N \rightarrow \infty$ . The problem may be solved numerically. Eleven plots of the oscillation function  $\delta(\Delta\tilde{\rho}, \theta)$  are drawn in figure 8, for angular deformation sectors including  $L$  samples. The displaced samples are located on these graphs using squares. The relative values of the radial displacements define optimal weighting windows that reduce the oscillations outside the deformation sector.

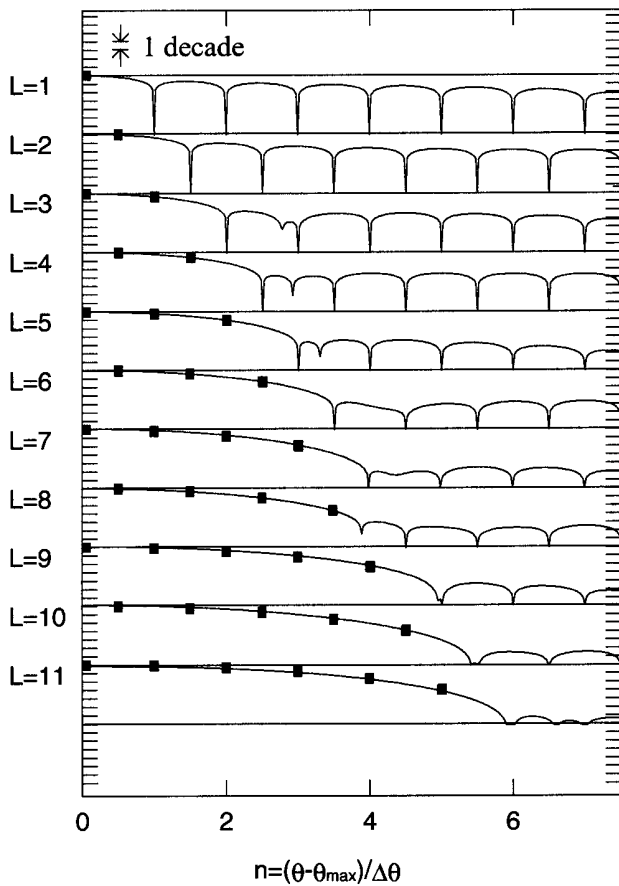
Table 1 gives the numerical values of these weighting coefficients. The left-hand column indicates the window width, or, alternately, the number  $L$  of displaced samples. The next columns show the ratio between the central displacement  $\Delta\rho_0$  and the  $n$ th neighbouring displacement  $\Delta\rho_n$ . Finally, the rightmost column contains the ratio between the central displacement and the maximum oscillation amplitude, for the corresponding window width.

All of the numerical values in table 1 are only slightly modified if  $N$  is finite. It has been checked that the differences are always less than 5% when  $N$  is greater than 16. Thus, the weighting windows can be used to control the contour deformation, following a local deformation source. Depending on the magnitude of the desired



**Table 1.** Numerical values of the weighting functions for  $N$  infinite.

$L$	$\Delta\rho_1/\rho_1$	$\Delta\rho_2/\rho_2$	$\Delta\rho_3/\rho_3$	$\Delta\rho_4/\rho_4$	$\Delta\rho_5/\rho_5$	$\Delta\rho_6/\rho_6$	$\Delta\rho_{\max}/\rho_{\max}$
1	—	—	—	—	—	—	4.7
2	0.788	—	—	—	—	—	13.5
3	0.429	—	—	—	—	—	144
4	0.860	0.223	—	—	—	—	440
5	0.587	0.093	—	—	—	—	3586
6	0.896	0.358	0.041	—	—	—	11 296
7	0.662	0.175	0.012	—	—	—	77 705
8	0.909	0.412	0.069	0.002	—	—	88 110
9	0.766	0.333	0.072	0.005	—	—	156 250
10	0.937	0.550	0.176	0.025	0.001	—	387 600
11	0.856	0.501	0.170	0.026	0.001	—	727 800

**Figure 8.** Oscillation functions  $\delta(\Delta\rho, \theta, L)$ .

deformation, different window widths can be used. The specific modelling technique decides what maximum width  $L$  is allowed for a given model, or, consequently, when the breakdown of a model occurs. In this case, a new model may be required, expressed with a larger number of parameters.

## 5. Application examples

Fourier–Shannon contour modelling allows the representation of a rich variety of geometric shapes. In this paper, we treat only the number of Fourier coefficients, considered as a global characteristic of the model. Although irregular-shape contours can be handled using other geometric interpolation and modelling techniques, the proposed model is particularly attractive for quasi-circular closed contours, since the number of Fourier coefficients is then drastically reduced. Thus, the geometric shape description becomes compact and easy to embed in another processing level, for example in a spatio-temporal model. Moreover, the knowledge of the frequency characteristics of the modelled contour also ensures the coherence between processing stages, from the signal processing point of view.

The Fourier–Shannon model was used to extract the boundary of the heart left ventricle (LV) from cardiac ultrasound images. The LV automatic detection procedures are generally based on modelling techniques, due to the various uncertainties encountered in the analysis of the echocardiographic images. The LV boundaries are not always distinguishable, due to the low image quality. This also occurs at the mytral valve level, when physical closed boundaries do not exist, for several intervals in the cardiac cycle.

The Fourier–Shannon technique is applied to model reference contours, traced by an expert and to data sets obtained with an automatic detection procedure. In the first case, the model uses rough data obtained from hand-drawn contours, and the result is a database with reference contours. In the second case, the Fourier–Shannon model is applied in conjunction with a discrete geometric active model, in order to detect the LV boundaries in sequences of images acquired during several cardiac cycles.

### 5.1. Modelling hand-drawn LV contours

The LV images were obtained using a trans-thoracic rotating probe with a high acquisition rate. The probe rotation movement combined with the heart dynamics

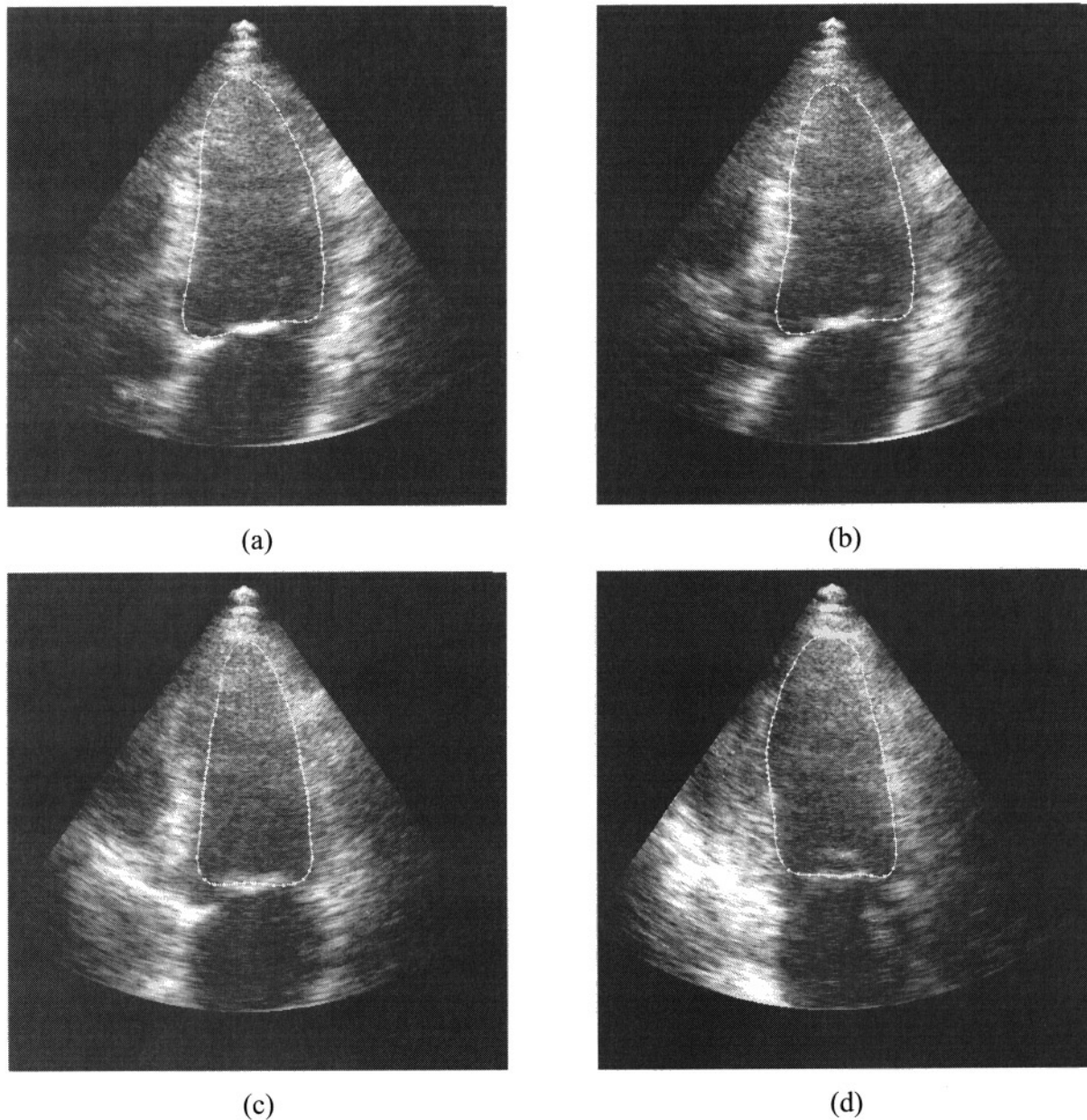


**Figure 9.** Four LV hand-drawn contour modelling.

produces significant difficulties for an expert to trace the LV boundaries. The inter-patient and inter-operator variability obtained after the analysis of several sequences of hand-drawn contours was found to be unacceptably high. In this context, a modelling approach was preferred. An interactive modelling software tool was designed for this purpose. The global model and the deformation technique were exploited to implement spatio-temporal coherence criteria, necessary to reduce expert variability [36, 37].

For the hand-drawn LV contours, initial data pre-processing was performed using standard smoothing and interpolation methods. The first processing step transforms

the rough dataset points into a polar development ( $\rho_n^d, \theta_n$ ) around their centre of inertia. The polar development set is then transformed into a continuous function (appendix B). After this initial modelling, the expert uses exclusively the local deformation technique detailed in section 4. Moreover, in the image sequence, the final contour of the previous image is used as an initial contour for the next image.

An example of the Fourier-Shannon LV contour modelling is shown on the image sequence of figure 9. Since the shape of the LV is regular, except for some rare pathologic cases, apical LV sections contain contours

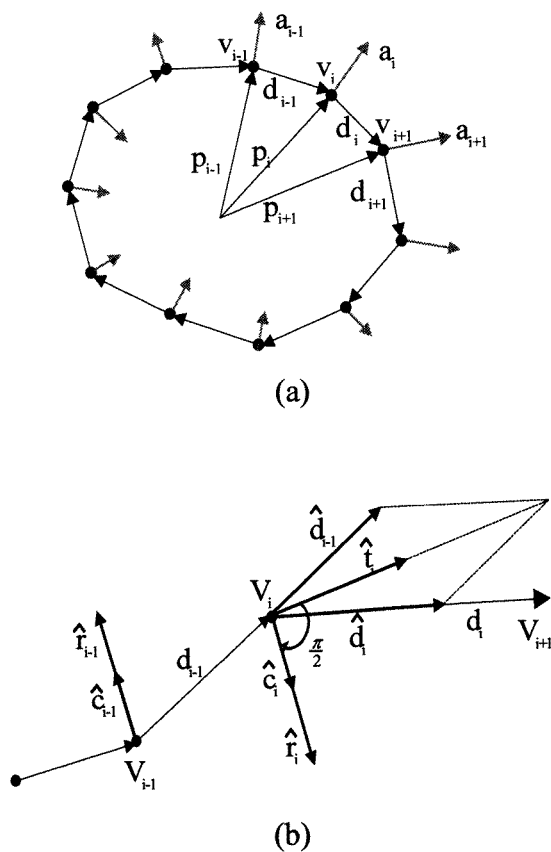


**Figure 10.** The discrete dynamic contour model. (a) The movement law of the contour edges ( $p_i$ , position;  $d_i$ , distance;  $v_i$ , velocity;  $a_i$ , acceleration). (b) The local coordinate system for a DDCM edge ( $r_i$  is the local normal vector given by the discrete local curvature  $c_i$ , and  $t_i$  is the local tangent vector at edge  $V_i$ ).

that produce relatively smooth polar developments. The images (a)–(d) in figure 9 are consecutive in a sequence obtained with the acquisition frequency of 42.74 images/s, the rotation speed of 8 rad/s and the spatial resolution of 0.02933 mm/pixel. The models are obtained from hand-drawn contours using  $N = 64$  characteristic samples and a maximum relative tolerance  $\varepsilon_T = 0.05$ . In the first image, an approximating contour of the LV was roughly drawn and was modelled with 64 characteristic samples. Then, this contour was deformed by the expert to obtain accurate matching with each piece of information in the sequence.

The deformation technique significantly helped the expert to deal in a coherent manner with the spatial and temporal constraints, required for a quality analysis of image sequences. This analysis was performed in order to obtain an accurate Fourier–Shannon model fitting for the LV boundaries using the cardiology expert knowledge.

## 5.2. Modelling automatic detected LV contours

In an automatic detection context, the model can be directly used to follow local image features. For an

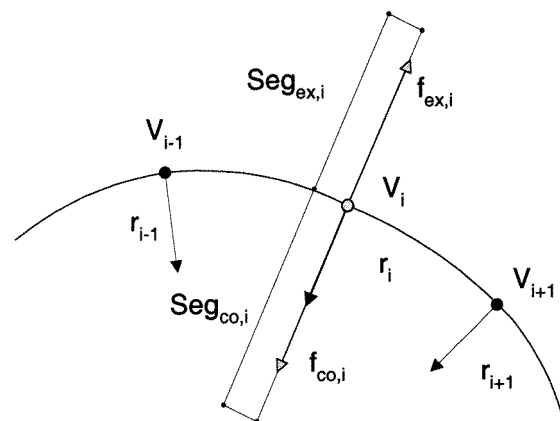


**Figure 11.** Compression and expansion segments and the associated external forces.

active Fourier–Shannon model, the contour is deformed in successive steps, using the weighting window introduced in section 4. Each deformation defines a new contour, which differs from the previous one within the sector of deformations, since the error due to the oscillations between the two contours outside this sector is reduced to the desired tolerance. A detailed presentation of the active Fourier–Shannon model will be the subject of a future work.

In this section, a preliminary study of the Fourier–Shannon model in an active detection environment is presented. The global model is used in conjunction with a discrete dynamic contour model (DDCM), detailed in [38], and adapted for ultrasound images of the heart in [36]. The aim of this study is to obtain a Fourier–Shannon evolution guided by local deformation sources.

The DDCM is a simple discrete model (figure 10) and its dynamic behaviour is driven by an explicit equilibrium between internal and external forces. Then, the force  $f_i$  acting on the  $i$ th edge of the DDCM is a combination of forces:

$$f_i = w_{ext} f_{ext,i} + w_{int} f_{int,i} + w_f v_i \quad (16)$$

$w_{int}$  and  $w_{ext}$  are positive weighting factors for the internal and external forces  $f_{int,i}$  and  $f_{ext,i}$ , respectively. The last term on the right-hand side of equation (16) is a viscosity-like force (weighted by  $w_f$ ), introduced to reduce the oscillations induced by the discrete-time dynamics around the equilibrium point.

Edge positions are determined, at each instant, by the movement laws

$$\begin{aligned} p_i(t + \Delta t) &= p_i(t) + v_i(t) \Delta t \\ v_i(t + \Delta t) &= v_i(t) + a_i(t) \Delta t \\ a_i(t + \Delta t) &= \frac{1}{m_i} f_i(t + \Delta t) \end{aligned} \quad (17)$$

where  $p_i$ ,  $v_i$ ,  $a_i$ , and  $m_i$  are the position, velocity, acceleration, and weight of edge  $V_i$ , respectively. The model dynamics is controlled by the time interval  $\Delta t$

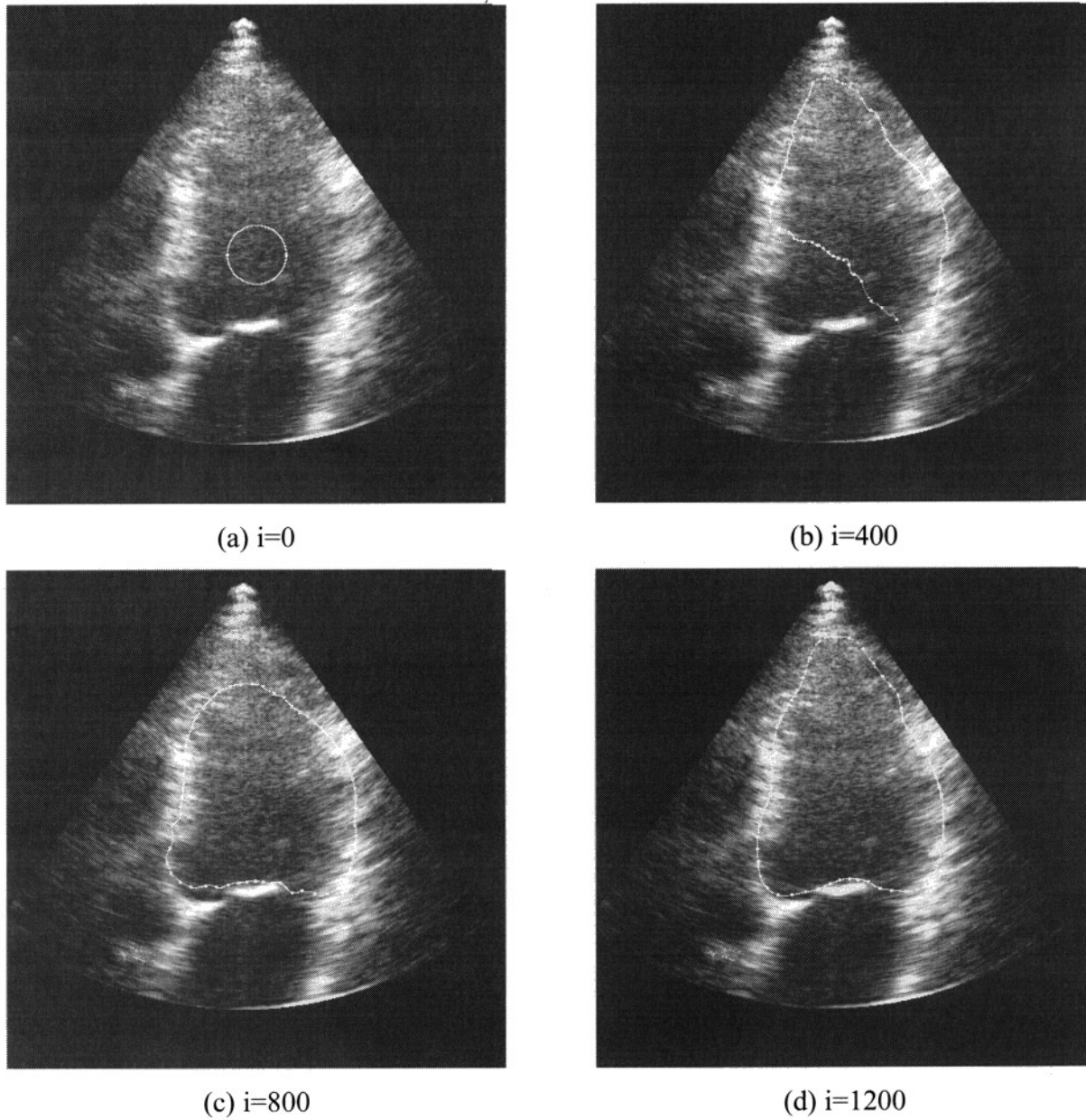


**Figure 12.** Fourier–Shannon modelling of the DDCM edge set during active deformation.  $i$  denotes the number of iterations ( $t = i \Delta t$  in (17)).

and by the  $m_i$  coefficients. We consider here that each edge has the same contribution to the contour deformation. Consequently, the  $m_i$  coefficients may be neglected.

The internal forces are computed using a minimal local elasticity constraint defined by

$$f_{int,i} \cdot \hat{r}_i = -\frac{1}{2}c_{i-1} \cdot \hat{r}_i + c_i \cdot \hat{r}_i - \frac{1}{2}c_{i+1} \cdot \hat{r}_{i+1} \quad (18)$$

where  $r_i$  is the local normal vector given by the discrete local curvature  $c_i$ .

The external force represents the energy of image features, and drives the deformation of the model. We use here the image grey level for simplicity of presentation,

along two radial segments associated to each edge  $V_i$  (figure 11). The image features are the average grey levels obtained for these segments. The external force amplitude is proportional to the difference between the average grey levels and its direction is given by the sign of this difference:

$$f_{ext,i} = f_{co,i} + f_{ex,i}$$

$$f_{co,i} = \frac{1}{\text{card}(\text{Seg}_{co,i})} \sum_{j \in \arg(P_j \in \text{Seg}_{co,i})} \|I(P_j)\| \cdot \hat{r}_i$$

$$f_{ex,i} = -\frac{1}{\text{card}(\text{Seg}_{ex,i})} \sum_{j \in \arg(P_j \in \text{Seg}_{ex,i})} \|I(P_j)\| \cdot \hat{r}_i. \quad (19)$$

Depending on the discrete curvature at each edge, the inward direction segment will produce a compression of the contour and the outward segment will produce an expansion of the contour (figure 11). More elaborate image features and faster DDCM dynamics are described in [36].

Both internal and external forces act exclusively along the radial direction [36, 38]. The DDCM edges move simultaneously following (16). After several iterations of the DDCM deformation algorithm, the edge set is globally modelled using the Fourier–Shannon technique described in section 3, with a given tolerance threshold. This method allows the study of the adequacy of the model for simultaneous local deformation sources. The overall contour evolution gives accurate information about the fitting capabilities of the Fourier–Shannon model in an active modelling environment. An example of the above technique is presented in figure 12.

The initial shape of the DDCM model is a circle with radius of 30 pixels. The force parameters are  $w_{int} = 1$ ,  $w_{ext} = 0.001$ , and  $w_f = 0.005$ . The external force  $f_{ext}$  is computed at each step using two 10-pixel width segments along the radial direction associated with the edge, following (18). The successive models obtained in figures 12 (b)–(d) using  $N = 64$  characteristic samples and a maximum relative tolerance  $\varepsilon_T = 0.01$  show a good agreement between the active and the Fourier–Shannon modelling techniques.

Both the above applications of the Fourier–Shannon model were integrated in a complex method, which proposes a spatio-temporal harmonic model for the restitution of the LV movement and deformations [36]. At certain stages, this method needs the expert-type information and uses a hand-drawn contour, modelled and adjusted as in section 3.1. This information is automatically distributed, following image sequence information, in the spatio-temporal modelling space, using the technique presented in section 5.1. The obtained contours are used as initial data for 3-D and 4-D restitution algorithms, also based on the Fourier coefficients characterization.

In this context, the link between different processing stages becomes essential for overall system efficiency. The harmonic description of the 2-D contours is the key mechanism that ensures the spatio-temporal coherence, required by the LV dynamics. Moreover, the specific relation between the heart movement and the acquisition probe movement/frequency produces explicit upper frequency bounds that must be considered in any accurate LV model. From this point of view, the Fourier–Shannon approach gives a direct solution, which guarantees that the obtained spatial and temporal model is error-free.

## 6. Conclusion

The approach described in this paper establishes the basis of the harmonic modelling of continuous contours. The Fourier–Shannon modelling technique proposes algorithms for determining the number of parameters needed for an accurate description of a continuous reference contour, and a local deformation technique designed for active modelling contexts. The model has several advantages, related mainly to the compact contour representation and to its intrinsic global modelling capabilities. It may be used in both static and active modelling environments, providing a solution for embedding *a priori* knowledge about the specific pattern recognition problem, like desired spatial accuracy and upper spatial and temporal frequency bounds. Moreover, this modelling technique allows complex geometric shape representation. The model is also well adapted for complex processing chains, where its dual continuous–discrete representation offers a flexible way of transferring information between system components. It is ideally suited for multi-scale/multi-resolution analyses.

The proposed methods were applied to obtain the contours of the left ventricle of the heart, from a sequence of ultrasound images. This is part of a project aimed at modelling the spatial and temporal deformations of the left ventricle using few cardiac cycles. The results presented here are used as a basis for the development of a complex LV tracking system, using both local image information and decision systems based on expert knowledge.

## Acknowledgment

The authors thank the ANVAR (Agence Nationale de Valorisation de la Recherche) for its involvement and financial support in this research project.

## Appendix A

This appendix details the computation of the sampling error estimate, in the case of a circular contour. If a circular contour of radius  $\rho_0$  is developed around an origin O very close to its centre C ( $|OC| = \Delta\rho \ll \rho_0$ ), a limited development around  $\Delta\rho/\rho_0 = 0$  can be considered:

$$\rho(\theta) = \rho_0 \left[ 1 + \frac{\Delta\rho}{\rho_0} \cos(\theta) - \frac{\Delta\rho^2}{2\rho_0} \sin^2 + \dots \right]. \quad (20)$$

This second-order approximated formula is used to calculate the sampling error defined by (9). Thus, it leads to

$$\varepsilon(k, \Delta\rho) = \max_n \left| 1 - \left[ 1 + \sum_{m=0}^{k-1} \{(\Delta\rho/\rho_0) \cos(m\Delta\theta) - (\Delta\rho^2/2\rho_0) \sin^2(m\Delta\theta)\} w^N(\theta, m, k) \right] \right|$$

$$\begin{aligned} & \times [1 + (\Delta\rho/\rho_0) \cos([n + \frac{1}{2}]\Delta\theta) \\ & - (\Delta\rho^2/2\rho_0) \sin^2([n + \frac{1}{2}]\Delta\theta)]^{-1} \end{aligned} \quad (21)$$

with  $0 \leq n < k$ , which yields equation (11):

$$\begin{aligned} & \varepsilon(k, \Delta\rho) \\ & = \max_n \left| 1 - \frac{1 + \sum_{m=0}^{k-1} (\Delta\rho/\rho_0) \cos(m\Delta\theta) w^N(\theta, m, k)}{1 + (\Delta\rho/\rho_0) \cos([n + \frac{1}{2}]\Delta\theta)} \right| \\ & \text{with } 0 \leq n < k. \end{aligned}$$

## Appendix B

The method used to obtain a smooth continuous contour starting from a rough dataset is detailed in this appendix. We suppose that the samples of an original contour are irregularly spaced. The initial collection of data points  $(\rho_n^d, \theta_n)$  is first transformed into a discrete function  $\rho_n(\theta_n)$  using the extension to the discrete case of a moving least-squares smoothing method, introduced by Papoulis in [39]. This technique uses a moving angular window of variable width  $\Delta\theta_n$ . The window is determined for each angular position  $n$  minimizing the root-mean-square (RMS) error between the corresponding data samples. The  $\Delta\theta_n$  expression in the continuous case is

$$\Delta\theta_n = 1.35 \left[ \frac{\sigma_B}{\rho_n''} \right]^{2/5} \quad (22)$$

where  $\rho_n''$  is the second derivative of  $\rho(\theta)$  evaluated for the central angle of the window  $\theta_n$ . In this discrete case,  $\rho_n''$  is estimated by the second derivative  $\hat{\rho}_n''$  of the parabola that provides a least-squares approximation of the samples.  $\sigma_B$  is estimated by the RMS deviation between these samples and the interpolation parabola  $\hat{\sigma}_B$ . In practice, both these estimations are computed using a window of any initial width (40% of the initial number of samples in our case). Then, an iterative algorithm is applied to find simultaneously  $\hat{\sigma}_B$ ,  $\hat{\rho}_n''$ , and  $\Delta\theta_n$ . Finally, an interpolation using cubic splines [40,41] is performed between these samples and a continuous contour  $\rho(\theta)$  is obtained. This contour can then be regularly sampled at a desired angular frequency.

## References

- [1] Staib L H and Duncan J S 1992 Boundary finding with parametrically deformable models *IEEE Trans. Pattern Anal. Machine Intell.* **14** 1061–75
- [2] Klingler J W, Vaughan C L, Fraker T D and Andrews L T 1988 Segmentation of echocardiographic images using mathematical morphology *IEEE Trans. Biomed. Eng.* **35** 925–34
- [3] Detmer P R, Bashein G and Martin R W 1990 Matched filter identification of left-ventricular endocardial borders in transesophageal echocardiograms *IEEE Trans. Med. Imaging* **9** 396–404
- [4] Feng J, Lin W-C and Chen C-T 1991 Epicardial boundary detection using fuzzy reasoning *IEEE Trans. Med. Imaging* **10** 187–99
- [5] Etoh M, Shirai Y and Asada M 1993 Active contour extraction based on region descriptions obtained from clustering *Syst. Comput. Japan* **24** (11) 55–65
- [6] Cox I J, Rehg J and Hingorani S 1993 A Bayesian multiple-hypothesis approach to edge grouping and contour segmentation *Int. J. Comput. Vision* **11** 5–24
- [7] Jiang H, Suzuki H and Toriwaki J 1993 A segmentation method based on region information and edge information *Syst. Comput. Japan* **24** (3) 48–58
- [8] Ueda N, Mase K and Suenaga Y 1993 A contour tracking method using an elastic contour model and an energy-minimisation approach *Syst. Comput. Japan* **24** (8) 59–70
- [9] Magnin I, Mathieu C, Friboulet D and Clarysse P 1993 Interêt de l'imagerie cardiaque 3D: acquisition, segmentation, quantification *Symp. Echocardiographie et Analyse d'Images Ventriculaires (Dijon, 1993)* pp 119–32
- [10] Nishimura T and Fujimoto T 1994 Fast contour line extraction algorithm with selective thresholding according to line continuity *Syst. Comput. Japan* **25** (3) 101–10
- [11] Geiger D, Gupta A, Costa L A and Vlontzos J 1995 Dynamic programming for detecting, tracking, and matching deformable contours *IEEE Trans. Pattern Anal. Machine Intell.* **17** 294–301
- [12] Cocquerez J-P and Philip S 1995 Analyse d'images: filtrage et segmentation ISBN 2-225-84923-4
- [13] Moritz W E, Pearlman A S, Mc Cabe D H, Medena D K, Ainsworth M E and Boles M S 1983 An ultrasonic technique for imaging the ventricle in three dimensions and calculating its volume *IEEE Trans. Biomed. Eng.* **BME-30** 482–91
- [14] Stickels K R and Wann L S 1984 An analysis of three-dimensional reconstructive echocardiography *Ultrasound Med. Biol.* **10** 575–80
- [15] McCann H A, Sharp J C, Kinter T M, Neill McEwan C, Barillot C and Greenleaf J F 1988 Multidimensional ultrasonic imaging for cardiology *Proc. IEEE* **76** 1063–71
- [16] Martin R W, Bashein G, Detmer P and Moritz W E 1990 Ventricular volume measurement from a multiplanar transesophageal ultrasonic imaging system: an *in vitro* study *IEEE Trans. Biomed. Eng.* **37** 442–8
- [17] Gustavsson T, Pasher R and Caidahl K 1993 Model based dynamic 3D reconstruction of the left ventricle from 2D cross-sectional echocardiograms *Comput. Med. Imaging Graphics* **17** 273–8
- [18] Cohen L D and Cohen I 1993 Finite-element methods for active contour models and balloons for 2-D and 3-D images *IEEE Trans. Pattern Anal. Machine Intell.* **15** 1131–47
- [19] Léger C, Thiel J, Bonciu C, Lédée R, Fantini J and Lamarque G 1993 Caractérisation d'une surface fermée convexe par interpolation de Shannon circulaire 4<sup>èmes</sup> Journées ORASIS (Mulhouse, 1993) pp 178–81
- [20] Lédée R, Léger C, Thiel J, Fantini J, Lamarque G, Bonciu C, Pottier J M and Marchal C 1994 Restitution volumique du ventricule gauche par sonde échocardiographique 2D tournante *Rev. Innovation Technol. Biol. Médecine* **15** 403–18

- [21] Coppini G, Poli R and Valli G 1995 Recovery of the 3D shape of left ventricle from echocardiographic images *IEEE Trans. Med. Imaging* **14** 301–17
- [22] Jerri A J 1977 The Shannon sampling theorem—its various extensions and applications: a tutorial review *Proc. IEEE* **65** 1565–96
- [23] Schanze T 1995 Sinc interpolation of discrete periodic signals *IEEE Trans. Signal Proc.* **43** 1502–3
- [24] Butzer P L 1983 A survey of the Whittaker–Shannon sampling theorem and some of its extensions *J. Math. Res.* **4** 185–212
- [25] Nashed M Z and Walter G G 1991 General sampling theorems for functions in reproducing kernel spaces *Math. Control, Signal, Syst.* **4** 363–90
- [26] Duda R O and Hart P E 1973 *Pattern Classification and Scene Analysis* (New York: Wiley)
- [27] Léger C, Thiel J, Lédée R, Patat F and Pourcelot L 1994 Modélisation de Fourier du contour parasternal du ventricule gauche *Traitement du Signal* **11** 155–69
- [28] Kass M, Witkin A and Tertzopolous D 1988 Snakes: active contour models *Int. J. Comput. Vision* **1** 321–31
- [29] Chakraborty A, Staib L H and Duncan J S 1996 Deformable boundary finding in medical images by integrating gradient and region information *IEEE Trans. Med. Imaging* **15** 859–70
- [30] Chalana V, Haynor D R and Kim Y 1994 Left-ventricular boundary detection from short-axis echocardiograms *Proc. SPIE Conf. on Medical Imaging* vol 2167, ed M H Loew (Bellingham, WA: SPIE) pp 786–94
- [31] Chalana V, Linker D T, Haynor D R and Kim Y 1996 A multiple active model for cardiac boundary detection on echocardiographic sequences *IEEE Trans. Med. Imaging* **15** 290–8
- [32] Duncan J S, Lee F A, Smeulders A W M and Zaret B L 1991 A bending energy model for measurement of cardiac shape deformity *IEEE Trans. Med. Imaging* **10** 307–20
- [33] Gunn S R and Nixon M S 1997 A robust snake implementation; a dual active contour model *IEEE Trans. Pattern Anal. Machine Intell.* **19** 63–8
- [34] Olstad B and Torp A H 1996 Encoding *a priori* information in active contour models *IEEE Trans. Pattern Analysis and Machine Intell.* **18** 863–72
- [35] Parker K J, Gao L, Lerner R M and Levinson S F 1996 Techniques for elastic imaging: a review *IEEE Eng. Med. Biol.* November/December 52–9
- [36] Bonciu CI 1997 4D reconstruction of the heart left ventricle using echocardiography images *PhD Thesis* Orleans University
- [37] Bonciu CI, Léger C, Lamarque G and Weber R 1998 4D visualization of the left ventricle using a rotating ultrasound probe during 4 cardiac cycles *Comput. Inform. Technol.* **6** (Special Issue on Biomedical Image Processing and Analysis) to appear
- [38] Lobregt S and Viergever M A 1995 A discrete dynamic contour model *IEEE Trans. Med. Imaging* **14** 12–24
- [39] Papoulis A 1977 *Signal Analysis* (New York: McGraw-Hill) pp 329–34
- [40] Unser M, Aldroubi A and Eden M 1992 Polynomial spline signal approximations: filter design and asymptotic equivalence with Shannon's sampling theorem *IEEE Trans. Inform. Theory* **38**
- [41] Press W H, Teukolsky S A, Vetterling W T and Flannery B P 1992 *Numerical Recipes in C. The Art of Scientific Computing* 2nd edn (Cambridge: Cambridge University Press)